

Simulation of Vehicle A-Pillar Aerodynamics of Various Yaw Angles

N.M. Murad¹, J. Naser¹, F. Alam² and S. Watkins²

¹School of Engineering and Science
Swinburne University of Technology, VIC, 3122 AUSTRALIA

²School of Aerospace, Mechanical and Manufacturing Engineering
RMIT University, VIC, 3083, AUSTRALIA

Abstract

Vortices formed around the A-pillar region dictate the pressure distribution on the side panels of a passenger vehicle and also can lead to aerodynamic noise generation. This paper analysed and compared qualitative flow visualization of airflow behavior based on the A-pillar region. Two simplified vehicle models with different A-pillar geometry were simulated using Computational Fluid Dynamics (CFD) under laboratory operating conditions. Commercial software (SWIFT) was used. In SWIFT, the simplified vehicle model was generated using Fame Hybrid. CFD simulations were carried out using SWIFT under steady state conditions using the HTM2 turbulence model. Investigations were carried out at velocities of 60, 100 and 140km/h and at 0, 5, 10 and 15 degree yaw angles. Results of C_p values were also compared against available experimental data. Results obtained using CFD modeling provided reasonable agreement against available experimental data.

Introduction

Vortices formed around the vehicle A-pillar region can lead to aerodynamic noise generation [3, 6]. Noise generated from the A-Pillar region is transferred to the passenger cabin causing annoyance and much discomfort to the vehicle occupants [3]. Over the years, research studies concerning A-pillar aerodynamics have focused mainly on understanding the mechanics of airflow behaviour when exposed to various A-pillar and windshield configurations to help further reduce aerodynamic noise. Previous research studies conducted, used predominantly experimental and/or numerical methods [1, 2, 3, 5, and 6].

Reviews from past literatures suggest that the key in A-pillar design to achieve low aerodynamic noise lies on having a slender A-pillar angle with round windshield radius. However, design and safety constraints damper this progress [1] and hence, current vehicle design still utilises the traditional A-pillar design with minimum windshield curvature giving it a quasi-sharp slanted edge shape. This type of design resulted in the generation of complex three-dimensional turbulent flow separation behind the A-pillar region.

In 2004, Murad [7] conducted a study of a simplified vehicle model with slanted edge A-pillar geometry design at 0-yaw angle using CFD simulation. The main reason of the study was to develop an appropriate numerical tool to capture the A-pillar vortex. From the study, Murad obtained reasonable result correlation with available experimental data and developed an appropriate numerical tool for studying A-pillar vortex by using CFD. Results from the study showed helical three-dimensional vortex generated behind the A-pillar region of the slanted edge model. The vortex close to the vehicle wall surface was elongated and spanned out diagonally following the A-pillar shape due to high values of Reynolds stresses in the U and W component of flow. The results also show high vortex intensity at

the base of the A-pillar, where the helical vortex originates, based on high amount of kinetic energy obtained at that region.

In this study, a simplified model with rectangular shaped A-pillar geometry at varying yaw angles similar to Alam [1] was simulated and qualitatively analysed in order to understand the mechanics of the airflow behaviour behind the rectangular A-pillar region. In addition, airflow behaviour behind a slanted A-pillar model, similar to Murad [7], at varying yaw angles was also simulated using CFD and qualitatively analysed. Surface coefficient of pressure (C_p) plots of both A-pillar models obtained through the CFD simulations were compared against available experimental data for validation purposes and to further assist in the understanding of A-pillar vortex behaviour close to the A-pillar/side window wall.

Vehicle Geometry and Boundary Conditions

Geometry configurations, boundary conditions and experimental data used in these simulations were obtained from Alam [1]. In his wind tunnel tests, Alam used a simplified model of a vehicle (40% scale) with varying windshield/A-pillar configurations. Two rows of pressure tapings (96.0 mm apart) were constructed close to the A-pillar region to capture static pressure values on the vehicle surface. The static pressure was then used to calculate the C_p values. Each row had 16 pressure tapping points, which were 32.0 mm apart. The simplified model was exposed to various flow velocities and yaw angles. In this study, CFD simulations were carried out on the rectangular edge A-pillar model at yaw angles of 0, 5, 10 and 15 degrees with respect to the tunnel in the computational domain, while simulations carried out on the slanted edge A-pillar model were at 5, 10 and 15 degrees yaw angles respectively. The commercial CFD package used for the simulations was SWIFT AVL. Fame Hybrid AVL was used as the grid generator.

Boundary conditions at the velocity inlet were set at 60, 100 and 140 km/h respectively (Correspond to Reynolds number of 2.169×10^6 , 3.615×10^6 and 5.061×10^6 respectively). The windshield for the rectangular edge model was 90 degrees from the vertical axis while on the slanted edge model, the windshield was at 60 degrees from the vertical axis.

For simulations in SWIFT, the calculation of kinetic energy and dissipation rate (k and ϵ) were based on the turbulence Intensity and turbulence length scale values of 1.8% and 5.8 mm (1.0% model height) respectively. The values for kinetic energy and dissipation rate varied accordingly with the inlet velocity.

Mesh Generation

Fame Hybrid in SWIFT uses an advance meshing system called the Arbitrary Cell Technology (ACT) where a blend of polyhedral grids was used to mesh and refine complex 3-D computational domain. An initial coarse mesh of around 250,000 grid cells were generated using Fame Hybrid. The final mesh

after refinement was slightly more than 1.0 million grid cells with a total of around 400,000 grid cells generated around the A-pillar region after refinement. Initial coarse surface mesh (100 mm in size) was generated on the wind tunnel wall. An initial surface mesh of 10 mm in size was generated on the vehicle model surface. A final surface mesh of 3.0 mm was generated around the A-pillar region after refinement. In addition, 10 boundary layer mesh were constructed from the model surface with each one measuring 2.0 mm in size. Grid independency test was performed after each grid refinements were made until error was restricted to a maximum of 5.0% relative to previous adaptation results.

Numerical Scheme and Strategy

In SWIFT, the calculation was first done using first order upwind scheme and central differencing scheme. Once convergence was reached, the AVL smart bound higher order scheme was then used. The convergence level for residuals was set to 0.1% with SIMPLE pressure-velocity coupling used together with 3-dimensional, steady and incompressible flow environment. Throughout the calculation, under-relaxation values were reduced whenever solution showed instability and divergence. The under-relaxation performed varied from one A-pillar model to the other. Turbulence models used in SWIFT was the Hybrid Turbulence Model 2 (HTM2).

Discussion of Results

CFD simulations on both the rectangular and slanted edge A-pillar models were carried out and Cp data values were obtained along the A-pillar region. Results from the Cp plots were within reasonable agreement with available experimental data.

Rectangular Model at 0-yaw angle

Results from relative pressure contour analysis showed that the A-pillar vortex increased in size and magnitude when exposed to an increase in velocity. At velocity of 100 km/h the A-pillar vortex appeared to be approximately 1/5 of the vehicle roof length. At 140 km/h, the A-pillar vortex appeared to be approximately 1/4 of the vehicle roof length.

Top view results of relative pressures contour showed a decrease in negative pressure magnitude along the y-axis (from A-pillar base to the roof). The area of separation at the A-pillar base was smaller and concentrated close to the A-pillar region due to its high intensity. The vortex expanded away from the side window and became larger as it moved upwards to a distance of approximately 2/3 from the base. At the same time the vortex core shifted downstream. As the vortex activity reached the roof of the model, the area of separation again became smaller and stretched. This resulted in the vortex core moving further downstream of the flow.

Top view results of turbulent kinetic energy contours showed a significant increase in magnitude at velocity of 140 km/h when compared to velocity at 60 km/h. At 140 km/h, high concentration of turbulent kinetic energy close to the A-pillar region but was decreasing in magnitude as it moved at 2/3 distance upwards from the base. As the A-pillar vortex mixed with separated flow from the roof region, it generated a high region of turbulent kinetic energy of similar magnitude to that at the base of the A-pillar region.

Further analysis from the Reynolds stress contours showed that the vortex was dominantly stronger in the vv' (y-direction) component followed by the ww' (z-direction) component. This was similar to the Reynolds stress component of the slanted edge

model at 0 yaw angle [7]. This showed that the A-pillar vortex was circulating diagonally and moving downstream to the flow. Surface streamline analysis of the rectangular model further showed that the A-pillar vortex reattachment region was around 45 degrees angle with respect to the A-pillar. This angle was halfway between the A-pillar and the vehicle bonnet. Surface streamline analysis by Murad [7] using the slanted edge model at 0 yaw also exhibited similar finding with the A-pillar vortex reattachment region at halfway (15 degrees) distance between the A-pillar and the vehicle bonnet (30 degrees).

Front view (z-axis) analysis of the CFD results taken of the turbulent kinetic energy contour showed that the airflow separation started from the corner between the bonnet and the A-pillar. As the airflow separated and started moving and circulating downstream to the rear of the vehicle, the vortex started to increase in size and evolved upwards until it reached the roof region of the vehicle (Figure 1). At the same time, the core of the A-pillar vortex was pushed outwards, away from the A-pillar. This phenomenon could be traced back due to the rectangular geometry of the A-pillar, forcing the A-pillar vortex to circulate at a steeper angle (45degrees) making it reach the roof region faster. In comparison, the A-pillar vortex of the slanted edge model at 0 degree yaw circulated downstream at a more acute angle. This resulted in a higher magnitude of turbulent kinetic energy (compared to the rectangular model) concentrated around a smaller region, placing the core of the A-pillar vortex closer to the driver/front passenger window.

CFD data analysis of Cp for the rectangular model taken along the bottom and top row region showed that the Cp values of the rectangular model showed a slow exponential decrease throughout the downstream region of the flow, a strong evidence of a large A-pillar vortex size surrounding much of the A-pillar and side window region. For the slanted edge model at 0 yaw angle, the Cp value plot for the bottom and top row region was more intense than the rectangular model but showed a faster exponential decrease throughout the downstream region of the flow, evidence of a smaller in size, but a more intense A-pillar vortex.

Rectangular Model at 5, 10 and 15 degrees yaw angles

Results from the rectangular model at varying yaw angles showed different characteristics to the rectangular model at 0 yaw angle. Different vortex size were developed on both sides of the A-pillar. In addition, results showed variations in vortex intensity at different yaw angle.

Top view results of turbulent kinetic energy contour for the 5, 10 and 15 degree yaw angle model showed that the A-pillar vortex formed around the vehicle A-pillar region at the windward side was smaller and compact in size due to the smaller area of separation and re-attachment downstream to the flow compared to the A-pillar vortex formed on the leeward side. Furthermore, the windward side exhibits a high magnitude in turbulent kinetic energy, with the A-pillar vortex core formed near to the A-pillar/side window region. On the leeward side, the A-pillar vortex core was formed further away from the A-pillar/side window region. Both A-pillar vortex on the windward and leeward side rotated in a clockwise direction (Figure 2). This is different from the model at 0 yaw angle where the vortex rotated in opposite direction to each other.

Front view results of relative pressure contour and streamline analysis showed that due to different yaw angles, the A-pillar vortex on the windward side was spread more towards the roof region next to the A-pillar and not much to the side window region. As the A-pillar vortex moved downstream, it became

larger in size, eventually connected with the turbulent boundary layer flow on the roof region and the A-pillar vortex on the leeward side. The A-pillar vortex on the leeward side originated from the A-pillar/bonnet corner region. As the flow moved downstream, flow separation evolved from the roof/side window region, eventually mixing with the flow separation from the A-pillar/bonnet region, resulted in a bigger A-pillar vortex. Relative pressure contour also showed very low pressure region downstream of the flow at area away from the A-pillar-side window, which also contained the core for the A-pillar vortex (Figures 3 & 4).

However, relative pressure contour analysis on the vehicle surface showed considerable high pressure spread on the vehicle wall. This phenomenon resulted from the thin viscous boundary layer effect developed close to the wall side window surface. On average, a C_p difference of -0.6 was observed between the low pressure region of the A-pillar vortex and the high pressure region of the boundary layer.

Reynolds stress analysis showed that the vortex on the windward and leeward side was stronger in the vv' and ww' component, evidence of the vortex moving and rotating downstream and upwards at approximately 45 degrees with respect to the A-pillar.

Results obtained from various yaw angles analysis of the rectangular model showed variations in vortex intensity. At 0 yaw angle, the vortex intensity was equally spread throughout the A-pillar/side window region. From the C_p analysis of the bottom and top row points, at 5 degree yaw, the windward side of the A-pillar started to show a steeper exponential decrease in C_p values during the first six bottom row points with a minimum of -1.50 before reaching a plateau. At 10 degree yaw, the C_p plot showed a steep exponential decrease during the first five bottom row points with a minimum of -1.51. At 15 degrees, a minimum of -1.0 was obtained from the first four points C_p plot of steep exponential decrease. This showed that as the yaw angle increased, the A-pillar vortex size on the windward side became smaller, resulting in an increase in vortex intensity, reaching peak intensity at 10 degree yaw before weakening back at 15 degree yaw. During this time, the leeward side experienced a steady exponential decline in vortex intensity with a leaner decline at every yaw angle increase. This is to further support the fact that the A-pillar vortex in the leeward side is bigger in size but smaller in intensity at the region close to the A-pillar/window area.

Slanted Edge Model at 5, 10 and 15 degrees yaw angles

Results from the slanted edge model at varying yaw angles also showed different characteristics to the slanted edge model at 0 yaw angle in that it exhibited A-pillar vortex at varying intensity and size on both sides of the A-pillar. The A-pillar vortex generated from the slanted edge model at varying yaw angle also showed several difference characteristics to the yawed rectangular model.

Top view (y-axis) CFD analysis of the relative pressure and turbulent kinetic energy contour showed that, due to the slanted edge geometry of the A-pillar, the A-pillar vortex intensity close to the A-pillar/side window wall was greater on the leeward side as oppose to the windward side on the rectangular model. The C_p data analysis showed a progressive increase in vortex intensity of the slanted edge model from 5 degree yaw angle until 15 degree yaw angle as oppose to a drop in vortex intensity at 15 degree yaw angle with the rectangular model. C_p data analysis also showed that with increase in vortex intensity, the vortex size at 5,

10 and 15 degree yaw angle on the leeward side was slightly smaller than the rectangular model. In addition, it was also observed that the A-pillar vortex formed at 5 and 10 degree yaw angle could only managed to sustain its intensity only for a short distance before reattaching itself to the side window wall but at 15 degree yaw angle, the separation area at low C_p values were spread out even much further downstream of the flow (Figure 5).

The front view relative pressure contour and streamline analysis showed that for the slanted edge model at various yaw angle, the airflow separation started on the side window on the windward side of the flow and not from the roof region as experienced by the rectangular model. On the leeward side, separation starts from the A-pillar to the side window. As the A-pillar vortex became larger downstream of the flow, it rotated beyond the boundary of the vehicle roof, mixing with turbulence boundary layer on the roof and reaching the A-pillar vortex on the windward side of the vehicle (Figure 6 & 7).

Reynolds stress analysis showed that the vortex on the leeward side was stronger in the uu' and ww' component, evidence that the vortex moved and rotated downstream and sideways. As the A-pillar vortex developed further and became established, the Reynolds stress analysis showed that the vv' and ww' component was stronger, evidence that the A-pillar vortex were rotating upwards and downstream to the flow. The A-pillar vortex on the windward side on the other hand, started of stronger in the vv' and ww' component and remained strong in that component all throughout the flow, evidence of the flow moving upwards and downstream to the flow.

Conclusions

A simplified vehicle model with rectangular and slanted A-pillar geometry was simulated and analysed to replicate flow behind a vehicle A-pillar region under laboratory operating conditions. Commercial CFD software, SWIFT was used for the simulations. In SWIFT, the simplified vehicle model was generated and meshed using Fame Hybrid. CFD simulations were carried out using SWIFT HTM2 turbulence model at steady state condition. Investigations were carried out at velocities of 60, 100 and 140km/h and at 0, 5, 10 and 15-degree yaw angle. Results showed that for the rectangular model, the A-pillar vortex generated was bigger in size when compared to the slanted edge model at 0 yaw but with less intensity. Results for the rectangular at various yaw angles showed that at the windward side, the A-pillar vortex generated had more intensity than the leeward side but was smaller in size. Results for the slanted edge model from various yaw angles showed that at the leeward side, the A-pillar vortex generated had a higher intensity and in size when compared to the A-pillar vortex in the windward side. Results for both model was greatly influenced by the yaw angles and also by the A-pillar geometry.

Acknowledgments

The authors would like to thank the Swinburne Centre for Astrophysics and Supercomputing for providing assistance with computing support and resources.

References

- [1] Alam, F., *The Effects of Car A-Pillar and Windshield Geometry and Yaw Angles on Local Flow and Noise: PhD Thesis*, RMIT University, Australia, 2000.
- [2] George, A.R., *Automobile Aerodynamic Noise, SAE Paper*, No 900315, 1990.
- [3] Hucho, W.H (editor), *Aerodynamics of Road Vehicles*, 2nd edn, Butterworths, London, 1998.

[4] Murad, N.M, Naser, J, Alam, F, Watkins, S, Simulation of Vehicle A-Pillar Aerodynamics using various Turbulence Models, *SAE Paper*, No 2004-01-0231, 2004.

[5] Popat, B.C., *Study of Flow and Noise Generation From Car A-Pillars: PhD Thesis*, University of London, 1991.

[6] Watkins, S., Gusts and Transients, in *Topics In Wind Noise and its Measurement Part 2-SP1457*, SAE, USA, 1999.

Appendices

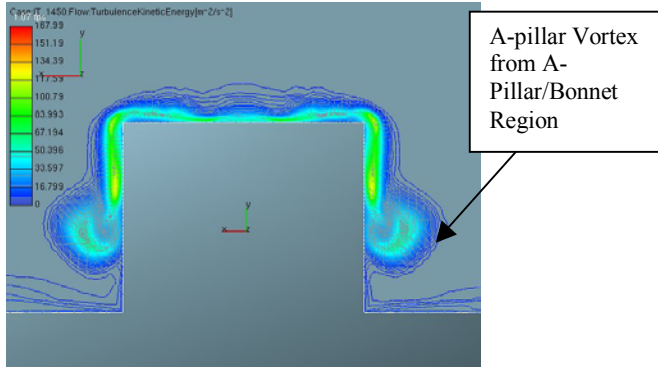


Figure 1. Front View (74 mm from Windshield) Turbulence Kinetic Energy Contour, Rectangular Model at 0 yaw, 140 km/h.

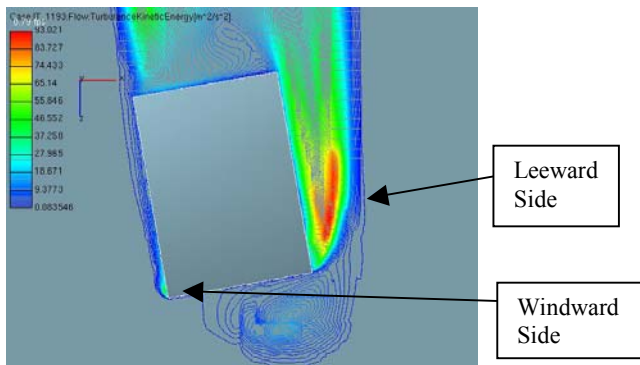


Figure 2. Top View (Bottom Row) Turbulence Kinetic Energy Contour, Rectangular Model at 10 yaw, 140 km/h.

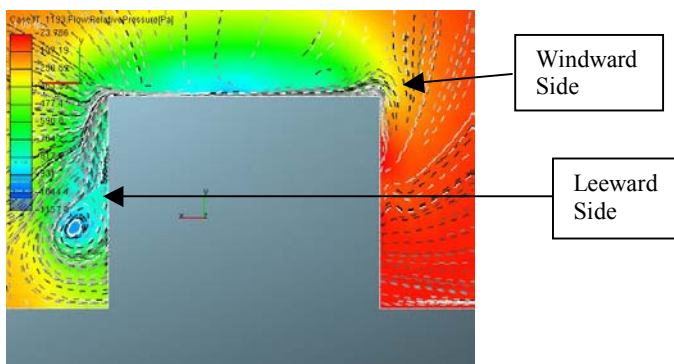


Figure 3. Front View (138 mm from Windshield) Relative Pressure Contour with Streamline, Rectangular Model at 10 yaw, 140 km/h.

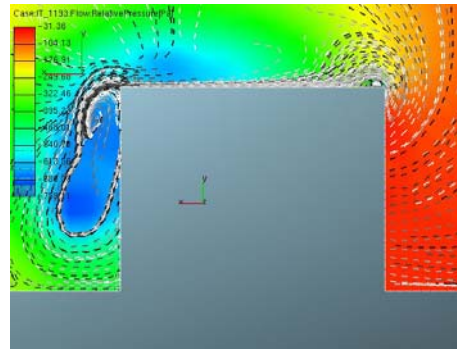


Figure 4. Front View (330 mm from Windshield) Relative Pressure Contour with Streamline, Rectangular Model at 10 yaw, 140 km/h.

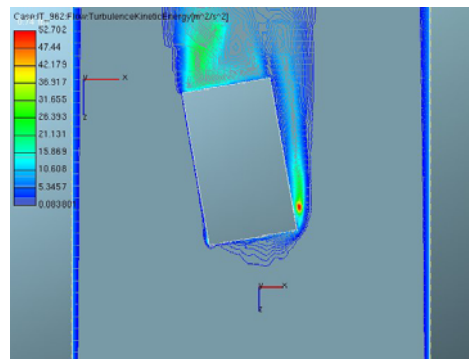


Figure 5. Top View (Bottom Row) Turbulence Kinetic Energy Contour, Slanted Edge Model at 10 yaw, 140 km/h.

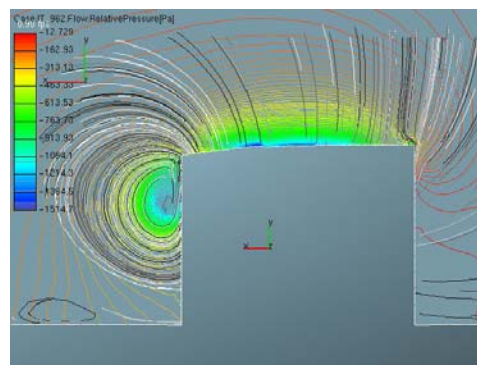


Figure 6. Front View (138 mm from Windshield) Relative Pressure Isolines with Streamline, Slanted Edge Model at 10 yaw, 140 km/h.

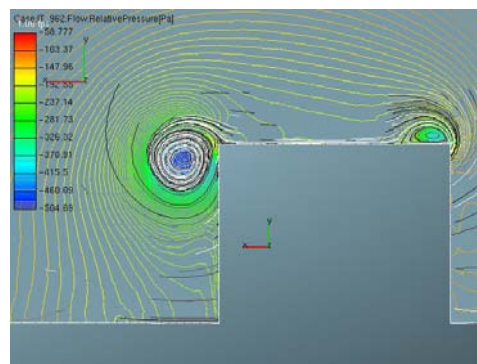


Figure 7. Front View (330 mm from Windshield) Relative Pressure Isolines with Streamline, Slanted Edge Model at 10 yaw, 140 km/h.